C-3 Alkyl/Arylalkyl-2,3-dideoxy Hex-2-enopyranosides as Antitubercular Agents: Synthesis, Biological Evaluation, and QSAR Study

Mohammad Saquib, Manish K. Gupta, Ram Sagar, Yenamandra S. Prabhakar,* Arun K. Shaw,* Rishi Kumar,[†] Prakas R. Maulik,[†] Anil N. Gaikwad, Sudhir Sinha, Anil K. Srivastava, Vinita Chaturvedi, Ranjana Srivastava, and Brahm S. Srivastava

Medicinal and Process Chemistry Division, Division of Molecular and Structural Biology, Drug Target Discovery and Development Division and Division of Microbiology, Central Drug Research Institute, Lucknow-226001, India

A series of C-3 alkyl and arylalkyl 2,3-dideoxy hex-2-enopyranoside derivatives were synthesized by Morita−Baylis−Hillman reaction using enulosides **4**, **5**, and **6** and various aliphatic and aromatic aldehydes. The compounds were evaluated *in vitro* for the complete inhibition of growth of *Mycobacterium tuberculosis* $H_{37}R_v$. They exhibited moderate to good activity in the range of 25−1.56 µg/mL. Among these, **4d**, **4h**, **5c**, and **4hr** showed activity at minimum inhibitory concentrations, 3.12, 6.25, 1.56, and 1.56 µg/mL, respectively. These compounds were safe against cytotoxicity in VERO cell line and mouse macrophage cell line J 744A.1. A QSAR analysis by CP-MLR with alignment-free 3D-descriptors indicated the relevance of structure space comparable to the minimum energy conformation (from conformational analysis) of **5c** to the activity. The study indicates that the compounds attaining the conformational space of **5c** and reflecting some symmetry, minimum eccentricity, and closely placed geometric and electronegativity centers therein are favorable for activity.

Introduction

Mycobacterium tuberculosis, the leading causative agent of tuberculosis (TB), is responsible for the morbidity and mortality of a large population worldwide. According to a WHO report, by 2020 AD nearly one billion more people will be infected, 200 million people will get sick, and 70 million will die from tuberculosis if proper steps are not taken to control it.[1−3] Moreover, the opportunistic TB infection due to AIDS and emergence of drug resistant TB strains have made its chemotherapeutic strategies increasingly ineffective.[4] Traditionally, it has relied heavily on a limited number of drugs such as isonicotinic acid hydrazide, rifampicin, ethambutal, streptomycin, ethionamide, pyrazinamide, fluoroquinolones, etc.[5] However, many of these drugs have different disadvantages such as prolonged treatment schedules, host toxicity, ineffectiveness against resistant strains, etc. This has motivated the search for new chemical prototypes capable of rapid mycobactericidal action with shortened duration of therapy, reduced toxicity, and enhanced activity against drug resistant strains and also against the latent bacteria for its control.[6−12] This paradigm shift in the strategies has drawn attention toward the outer cell wall and membranes of the pathogen as an attractive target for exploring new drugs.[13,14] In mycobacteria, the cell wall structure consists of a dense network of cross-linked sugar residues esterified with mycolic acid at the ends.[15,16] This understanding has prompted the investigation of various sugar prototypes with distinct characteristics as potential antitubercular agents.[17−21] Earlier, we investigated some highly functionalized heptenol and octenol derivatives from glucal and galactal for their antitubercular activity.[22,23] A quantitative structure−activity relationship (QSAR) study of these analogues with topological descriptors has suggested less branched and saturated structural templates for improved activity.[24] In recent literature, some 2*H*-pyran-3(6*H*)-one derivatives (Figure 1) are reported to exhibit significant activity against Gram-positive bacteria.[25] A variety of carbohydrate derivatives are also known to interfere with the cell wall biosynthesis of *M. tuberculosis*.[6,19,20] These studies suggested that arabinogalactan-linked disaccharides and decaprenol phosphoarabinosides interfere with the mycobacterial arabinosyltransferases. Moreover, some iminosugars are inhibitors of UDPGal*f* transferase,[a] in mycobacterial cell wall biosynthesis.[21] All these studies emphasize modified carbohydrates as potential scaffolds to interfere with the components of mycobacterial cell wall biosynthesis. In these background studies, C-3 alkyl and arylalky 2,3-dideoxy hexenopyranosides were synthesized to investigate their activity against *M. tuberculosis* and to develop a rationale for the activity. In recent modeling studies, the alignment-free 3D-descriptors from the molecular geometry were increasingly put to use as an alternative to the grid-based 3D-QSAR studies.[26−33] They offer insight to the receptor via the conformational space of the probe molecules and are successfully used in the development of rationales for divergent biological activities including tuberculosis.[27,29,31−35] In view of this, a QSAR of antitubercular activity of these hexenopyranosides is attempted using the alignment-free 3D-descriptors from DRAGON software.[36]

Chemistry. The synthesis of prototype molecules in this study was initiated with 3,4,6-tri-*O*-acetyl-α-D-glucal (**1**).[37] Iodine-catalyzed Ferrier rearrangement[38,39] of **1** with isopropanol furnished 4,6-di-*O*-acetyl-2,3-dideoxy hex-2-enopyranoside (**2**). Its deacetylation yielded dihydroxy derivative **3**, which upon allylic oxidation[40] followed by acylation of C-6 hydroxyl with different acylchlorides resulted in **4**, **5**, and **6** in good yields (Scheme 1).

* To whom correspondence should be addressed. (Y.S.P.) Phone:+91-522-2612411; fax:+91-522-2623405; e-mail: yenpra@yahoo.com. (A.K.S.) Phone:+91-522-2612411; fax: +91-522-2623405; e-mail: akshaw55@yahoo.com.
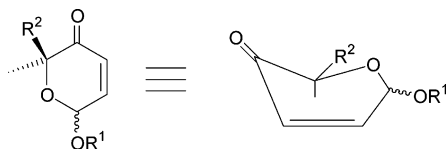
† R.K. and P.R.M. provided X-ray crystal data.

Figure 1. Substituted-2*H*-pyran-3(6*H*)-ones associated with activity against Gram-positive bacteria; R^1 and R^2 are alkyl and aryl groups, respectively.

The Morita−Baylis−Hillman (MBH) reaction[41−43] of **4**, **5**, and **6** with various aliphatic and aromatic aldehydes in the presence of TiCl₄/TBAI in DCM at −78 to −30 °C yielded highly diastereoenriched **4a−h**, **5c**, and **6c−h** (Scheme 2). The reaction is almost completely diastereoselective (>99%) without using any chiral catalyst. It is due to the formation of an ortho-ester intermediate during the reaction.[44] Making use of our previously reported procedure,[44] the C-4 keto group of **4a−f**, **4h**, **5c**, **6c**, **6f**, and **6h** were stereoselectively reduced with NaBH₄ in the presence of CeCl₃·7H₂O, leading to the formation of their *erythro* derivatives, **4ar−fr**, **4hr**, **5cr**, **6cr**, **6fr**, and **6hr**, respectively, in very good yields (Scheme 2). All the compounds were purified by column chromatography and characterized by elemental analyses, IR, NMR, and FABMAS spectra.

Among the analogues, the crystals of **4dr** were obtained on slow evaporation of its solution in acetone−hexane (1:3) at room temperature. Figure 2 is the *ORTEP* diagram of **4dr** from the X-ray study. It crystallized in monoclinic form with $P2_1$ space group. The central hexenopyranose ring is in a distorted half chair conformation with unsaturation between C-2 and C-3. In the Cahn−Ingold−Prelog system,[45] the relative conformations of C-1, C-4, C-5, and C-1′ are assigned as *S*, *S*, *R*, and *R*, respectively.

Biology. The compounds were evaluated for their *in vitro* antitubercular activity against *M. tuberculosis H₃₇Rv* in Agar dilution assay.[46] The minimum concentrations of the compounds required for the complete inhibition of the bacterial growth per spot (minimum inhibitory concentration, MIC) are summarized in Table 1. Ofloxacin was used as the standard drug (MIC is 0.75 μg/mL). Among these analogues, **4d**, **4h**, **5c**, and **4hr** showed activity at MICs 3.12, 6.25, 1.56, and 1.56 μg/mL, respectively.

Cytotoxicity was investigated for **4d**, **4h**, **5c**, and **4hr** in VERO cell line[47] and in mouse macrophage cell line J 744A.1.[48] In VERO cell line, **4h**, **5c**, and **4hr** showed cytotoxicity at 25 μg/mL and **4d** showed no toxicity even at 100 μg/mL. In mouse macrophage cell line J 744A.1 assay, the compounds were tested at 12.5, 25, and 50 μg/mL, in parallel with standard antitubercular drugs, Rifampicin and Sparfloxacin. These compounds did not show any toxicity.

QSAR. The QSAR study was attempted with two structure databases representing the X-ray structure **4dr** (Figures 2, 3a) and the conformational analysis-derived minimum energy structure of a high active compound **5c** (Figure 3b). The conformational space of these two structure databases differ in their C-3 substitution region (Figure 3). Alignment-free 3D-descriptors from DRAGON software[36] were opted as indices of the conformational space. It resulted in 681 and 679 descriptors, respectively, for **4dr** and **5c** databases. The computational procedures of embedded structural information divide these indices into eight descriptor classes.[36]

The QSAR models have been developed using CP-MLR (combinatorial protocol in multiple linear regression) in conjunction with a three-stage descriptor classification protocol.[49,50] CP-MLR is a variable selection procedure for the model development.[49−51] The descriptor classification protocol[50] typi-

cally segregates the descriptor classes into four categories depending on the significance of information content to the activity (Figure 4). The first three categories are primary contributors (category I: a descriptor class forming a model with its constituent descriptors), collective contributors (category II: a descriptor class unable to form a model with its constituent descriptors alone, but can form model(s) in combination with a descriptor from another such class), and secondary contributors (category III: a descriptor class forming model(s) only in combination with the category I). The last category is noncontributors, a descriptor class not forming a model in any manner such as in categories I, II, or III. The descriptor classes provide scope to understand the phenomenon under investigation in relation to the concepts embedded in them.

Results and Discussion

Among the highly active analogues, **4d** carries a trimethylacetyl protection group at the C-6 position and a *p*-cyanophenyl methyl side chain at the C-3 position of hexenopyranoside ring. In **4d**, the replacement of C-3 *p*-cyanophenyl methyl group by a *p*-nitrophenyl methyl (**4c**) or decyl moiety (**4h**) has resulted in lowering the activity of the corresponding analogues. Compound **5c**, a C-6 acetyl variant of **4c**, showed remarkably high activity (1.56 μg/mL). However, in these analogues, replacement of the C-6 trimethylacetyl or acetyl by a *p*-nitrobenzoyl group resulted in loss of their antitubercular activity (**6c−h**).

The compound **4hr** formed by the reduction of the C-4 carbonyl of **4h** showed better antitubercular activity (1.56 μg/mL) than **4h** itself (6.25 μg/mL). However, the other reduced compounds (e.g., **4dr** and **5cr**) were found to be far less active than their precursors. In the case of compounds with a C-6 *p*-nitrobenzoyl group, the C-4 carbonyl reduction has little effect on the activity. For example, **6cr**, **6fr**, and **6hr** showed almost the same activity as **6c**, **6f**, and **6h**. These results thus suggest that in 2,3-dideoxy hexenopyranosides, the nature of the side chain at C-3 and the protection group at C-6 play an important role in determining the antitubercular activity of these compounds.

QSAR Analysis. The alignment-free 3D-descriptors of X-ray crystal structure (**4dr**) database of hexenopyranosides (Table 1) did not lead to any model for the antitubercular activity. Under identical conditions, three 3D-descriptors classes, namely GEO (geometrical descriptors),[36] WHIM (weighted holistic invariant molecular descriptors),[26] and GETAWAY (geometry, topology, and atom-weights assembly descriptors)[30,31] of the minimum energy conformation of high active compound **5c** have evolved as collective contributors (category II) to explain the activity. At the end of a search for four parameter models, 50 descriptors (Table 2) have emerged from these descriptor classes to model the activity. The following are selected three- and four-parameter models[52] for the activity from a pool of equations.

$$-\log \text{MIC} = -3.667(0.558)\text{PJI3} - 5.204(2.110)\text{E3v} + 11.832(3.735)\text{R1u}^+ + 7.654$$
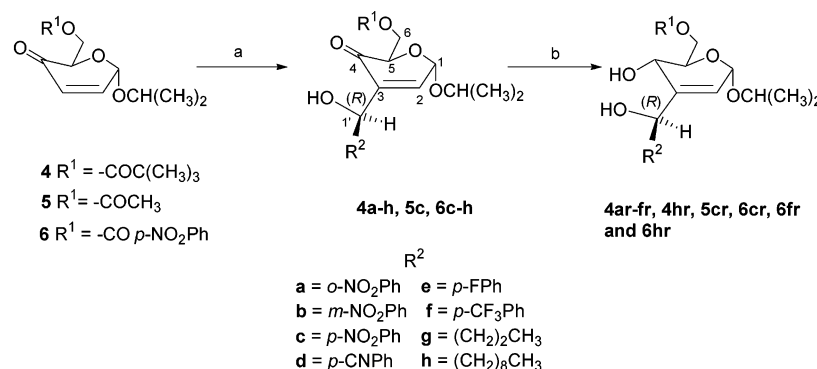
$$n = 23, r = 0.835, Q^2 = 0.508, s = 0.251, F = 14.61 \quad (1)$$

$$-\log \text{MIC} = -3.571(0.518)\text{PJI3} - 14.986(4.940)\text{ISH} + 40.044(10.726)\text{HATS2p} - 59.740(17.397)\text{R6e}^+ + 19.290$$

$$n = 23, r = 0.879, Q^2 = 0.573, s = 0.224, F = 15.23 \quad (2)$$

Scheme 1[a]
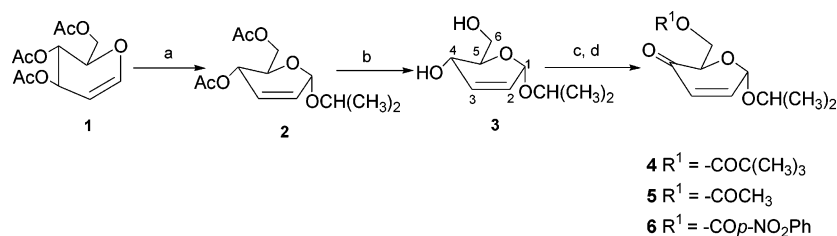
[a] Reagents: (a) $(CH_3)_2CHOH$, THF, I_2, 3 h, rt; (b) NaOMe, MeOH, 2 h, rt; (c) MnO_2, $CHCl_3$, 48 h, rt; (d) $(CH_3)_3CCOCl/(CH_3CO)_2O/p\text{-}O_2N\text{-}Ph\text{-}COCl$, pyridine, 6−48 h, 0−5 °C.

Scheme 2[a]

4 R^1 = -$COC(CH_3)_3$
5 R^1= -$COCH_3$
6 R^1 = -$CO\ p\text{-}NO_2Ph$

4a-h, 5c, 6c-h

4ar-fr, 4hr, 5cr, 6cr, 6fr
and 6hr

R^2
a = $o\text{-}NO_2Ph$ e = $p\text{-}FPh$
b = $m\text{-}NO_2Ph$ f = $p\text{-}CF_3Ph$
c = $p\text{-}NO_2Ph$ g = $(CH_2)_2CH_3$
d = $p\text{-}CNPh$ h = $(CH_2)_8CH_3$

[a] Reagents: (a) $TiCl_4$, TBAI, R^2CHO, DCM, 8−48 h, −78 °C → −30 °C; (b) $NaBH_4$, $CeCl_3 \cdot 7H_2O$, C_2H_5OH, 2−5 h, rt.
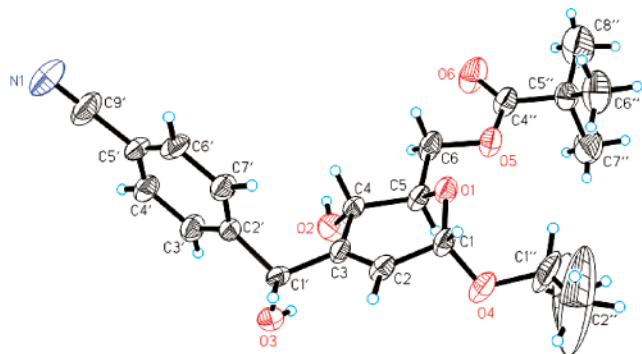
Figure 2. The *ORTEP* diagram (30% probability) of **4dr** with atomic numbering scheme.

In the randomization study, none of the identified models has shown any chance correlation. These are further validated through two test sets corresponding to descriptor clustering and random selection procedures with each one containing eight out of twenty-three compounds of Table 1. The test sets predictions are in agreement with their experimental values (Table 3; Figure 5).

Among the descriptors, PJI3 (3D Petitjean shape index; GEO class) has the highest influence on the activity of these analogues. It is a measure of eccentricity in the molecules. Its regression coefficient suggests that molecular structures with compact conformational features are favorable for activity. In eq 1, E3v is a directional WHIM descriptor for axial density (v; weighted by atomic van der Waals volumes) along principal axes 3. Its regression coefficient suggests in favor of reduced axial density for enhancement in activity. The GETAWAY descriptors ISH, R1u+, R6e+, and HATS2p (eqs 1 and 2) are embedded with the information from the molecular influence matrix (MIM, H-matrix). In this class, ISH (standardized information content on the leverage equality) encodes molecular symmetry information. It suggests in favor of symmetry in molecules for better activity. The descriptors R1u+ and R6e+,

Table 1. Observed and Predicted Antitubercular Activity of 2,3-Dideoxy Hexenopyranosides (Scheme 2)

compd no.	MIC[a] (μg/mL)	−log MIC[b]			
		obsd	eq 1	eq 2	PLS
4a	50	3.93	4.05	3.78	4.03
4b	50	3.93	4.06	4.2	3.87
4c	50	3.93	4.29	4.29	4.11
4d	3.12	5.11	4.54	4.66	4.83
4e	NA		4.15	4.27	4.15
4f	50	3.95	4.12	4.08	4.04
4g	25	4.14	3.98	4.03	4.34
4h	6.25	4.83	5.02	5.05	5.02
5c	1.56	5.39	4.94	4.99	5.03
6c	25	4.29	4.08	4.1	4.38
6d	25	4.27	4.46	4.78	4.66
6e	25	4.26	4.16	4.08	4.16
6f	25	4.31	4.13	4.18	4.36
6g	25	4.21	4.47	4.17	4.04
6h	25	4.29	4.38	4.49	4.25
4ar	25	4.23	4.28	3.99	4.00
4br	25	4.23	3.87	3.97	3.94
4cr	NA	-	4.44	4.55	4.3
4dr	NA	-	4.60	4.76	4.85
4er	25	4.20	4.45	4.35	4.28
4fr	25	4.25	4.08	4.31	4.07
4hr	1.56	5.44	5.00	4.92	5.19
5cr	25	4.18	4.90	4.46	4.46
6cr	25	4.29	4.17	4.54	4.56
6fr	25	4.31	4.14	4.03	4.26
6hr	25	4.30	4.36	4.38	4.39

[a] NA: not active up to 50 μg/mL. [b] MIC is in moles per liter.

respectively, represent the influence of maximal autocorrelations of lag 1 (u; unweighted) and lag 6 (e; weighted by atomic Sanderson electronegativities) of R-matrix (MIM as a fraction of distance matrix) on the activity. The descriptor HATS2p is autocorrelation of lag 2 (p; weighted by atomic polarizabilities) from the MIM. The regression coefficients of these descriptors suggest in favor of increasing number of one- and two-centered fragments in the chosen molecular conformation for better activity. Besides the three- and four-descriptor equations, a
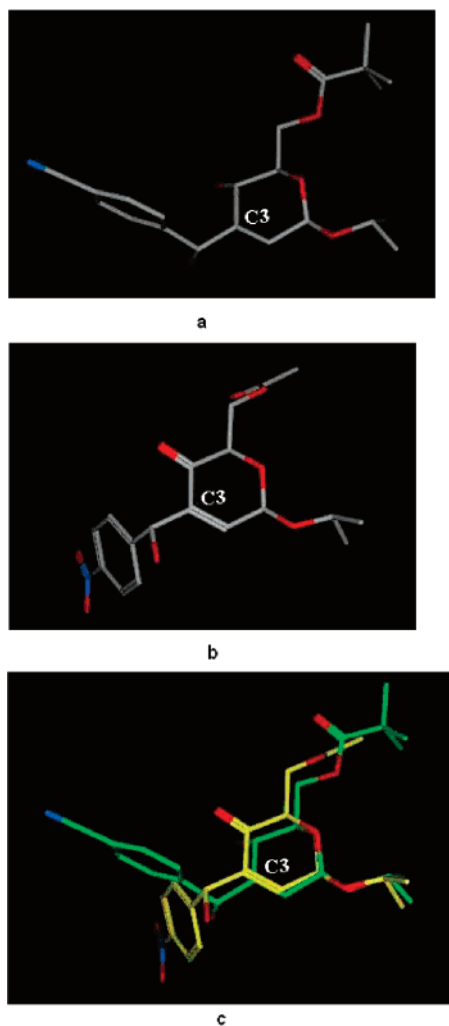
Figure 3. (a) X-ray structure of **4dr**; (b) conformational analysis derived minimum energy structure of **5c**; (c) superimposition pose of **4dr** (carbons: green) and **5c** (carbons: yellow); in all, oxygens are in red and nitrogens are in blue; hydrogens are suppressed for clarity.

Figure 4. Schematic representation of categorization of descriptor classes. A, B, C, etc., in circles are descriptor classes, and a_i, b_i, c_i, etc., respectively, are their constituent descriptors. Depending on the information content to correlate the activity, the descriptor classes are put into four categories as primary contributors (category I), collective contributors (category II), secondary contributors (category III), and non-contributors (category IV). Coefficients of a_i, b_i, c_i, etc., are not shown.

number of higher models also exist among the identified descriptors (Table 2).

A PLS (partial least-squares) analysis has been carried out on these 50 CP-MLR identified descriptors (Table 2) to facilitate the development of a 'single window' structure−activity model. In the PLS cross-validation,[53] three components are found to be the optimum for these 50 descriptors (dataset-I) and they explained 76% variance in the activity ($r = 0.872$, $Q^2 = 0.588$, $s = 0.223$, $F = 20.20$). A PLS analysis has also been carried out on the dataset devoid of these 50 identified descriptors (dataset-II; 629 descriptors). Under identical conditions, the dataset-II could explain only 63% variance in the activity ($r = 0.794$, $Q^2 = 0.345$, $s = 0.278$, $F = 4.55$). The dataset of 681 descriptors of the X-ray structure (**4dr**) database has resulted in a far inferior PLS model and explained only 57% variance in the activity ($r = 0.758$, $Q^2 = 0.264$, $s = 0.298$, $F = 8.54$). These results clearly substantiate the relevance of the 50 identified descriptors (Table 2) in modeling the activity of these compounds. The MLR-like PLS coefficients of these 50 descriptors are given in Table 2. Figure 6 shows a plot of the fraction contribution of normalized regression coefficients of these descriptors to the activity (Table 2).

The PLS analysis has also suggested that PJI3 is the most determining descriptor for modeling the activity of the com-
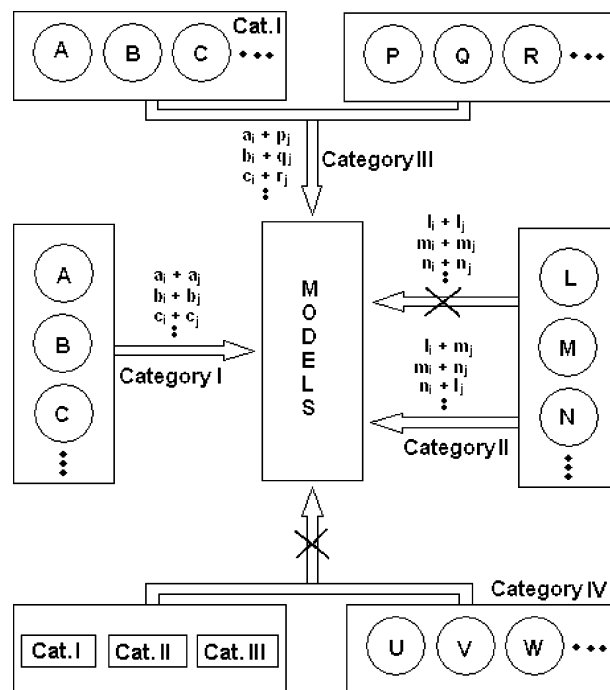
pounds (Table 2; descriptor no. 3 in Figure 6). The other significant descriptors in the PLS model are SPH, DISPe (GEO), Gu, G1v, G3v, L3u, E3e (WHIM), ISH, and R3m+ (GETAWAY) (Table 2; descriptor nos. 2, 5, 18, 11, 12, 9, 14, 19, and 40 in Figure 6). Among them, SPH (spherosity) is an anisometry descriptor and DISPe is a COMMA2[28] descriptor. The coefficient SPH suggests in favor of flat molecules for the activity. DISPe is a measure of displacement between the geometric and the electronegativity (e) centers in the molecule. Its negative regression coefficient suggests that an increasing separation between geometric and electronegativity centers is detrimental to the activity.

Both ISH (GETAWAY) and Gu (global molecular symmetry, unweighted; WHIM) infer about molecular symmetry (eq 2; Table 2). They suggest in favor of symmetry in the compounds for the activity. The directional WHIM descriptors G1v, G3v, L3u, and E3e (weighted by v, u, or e) represent the projections of symmetry (G), dimension (L), and density (E) of the atoms along respective principal axis 1, 2, or 3. Among these, the coefficients of G1v, G3v, and L3u (Table 2) suggest in favor of larger 1 and 3 axial symmetries and dimension for better activity. The coefficient of E3e (Table 2) suggests a reduced axial density, weighed by electronegativity. The descriptor R3m+ (GETAWAY) is R maximal autocorrelation of lag 3 weighted by atomic mass (m). Its coefficient (Table 2) suggests three-centered structural fragments with minimum atomic masses. Collectively, the analysis suggests that minimizing of PJI3, SPH, DISPe, Gu, E3e, ISH, and R3m+ and maximizing of G1v, G3v, and L3u in the compounds would lead to improved activity. In terms of molecular features, an extended structural frame, reduced symmetry, and separation in geometric and electronegativity centers are detrimental to the activity. At the same time the compounds with conformational features of

Table 2. The Identified 3D-Descriptors of Minimum Energy Conformation (**5c**)-Directed Structure Database of 2,3-Dideoxy Hexenopyranosides (Table 1) for Modeling Their Antitubercular Activity

no.	descriptor[a]	regr coeff (fc) order[b]
	Geometrical	
1	SPAM	0.281(0.005)45
2	SPH	−1.760(−0.054)3
3	PJI3	−1.411(−0.109)1
4	DISPm	−0.006(−0.020)16
5	DISPe	−0.441(−0.042)6
6	DISPp	−0.046(−0.007)38
7	G(N..F)	0.001(0.009)37
	WHIM	
8	L1u	−0.010(−0.015)24
9	L3u	0.120(0.039)7
10	L1v	−0.008(−0.014)26
11	G1v	16.783(0.056)2
12	G3v	9.568(0.036)9
13	E3v	−0.622(−0.013)28
14	E3e	−1.148(−0.038)8
15	L1p	−0.008(−0.013)29
16	G2p	1.283(0.006)42
17	Tp	0.001(0.002)47
18	Gu	−16.095(−0.048)4
	GETAWAY	
19	ISH	−6.043(−0.044)5
20	HIC	0.019(0.003)46
21	H6u	0.051(0.010)31
22	HTu	0.002(0.009)35
23	HATS0u	0.505(0.010)33
24	HATS6u	−0.844(−0.019)17
25	HATS0v	3.705(0.030)11
26	HATS1v	2.745(0.018)18
27	H6e	0.026(0.005)44
28	HATS6e	−0.669(−0.016)22
29	H1p	0.169(0.009)36
30	HATS0p	3.732(0.027)15
31	HATS1p	3.018(0.018)19
32	HATS2p	0.095(0.001)49
33	HATS3p	−2.052(−0.014)27
34	R2u	0.049(0.005)43
35	R3u	0.097(0.012)30
36	R6u	−0.023(−0.002)48
37	R1u+	2.388(0.029)12
38	R1m+	0.587(0.017)21
39	R2m+	−0.562(−0.016)23
40	R3m+	−5.194(−0.031)10
41	R6m+	−1.785(−0.007)41
42	RTm+	0.482(0.014)25
43	R2v+	2.188(0.007)39
44	R3e	0.110(0.010)32
45	RTe	−0.0002(−0.0003)50
46	R2e+	−0.826(−0.017)20
47	R3e+	−3.823(−0.028)14
48	R6e+	−8.606(−0.029)13
49	R1p	0.267(0.009)34
50	R2p+	2.188(0.007)40

[a] Geometrical: SPAM, average span sphere radius; SPH, spherosity; PJI3, 3D Petitjean shape index; DISP*w*, displacement between the geometric center and the center of the *w* property field, calculated with respect to the molecular principal axes, the last character '*w*' refers to the weighting property which may be either '*m*' for atomic masses or '*v*' for atomic van der Waals volumes or '*e*' for Sanderson electronegativities or '*p*' for atomic polarizabilities or '*u*' for unweighted; G(N..F) sum of geometrical distances between N and F. WHIM: L*nw*, G*nw*, and E*nw*, directional indices of size, symmetry, and accessibility, respectively; in this, *n* refers to the directional component 1, 2, or 3, and '*w*' refers to the weighting property (for '*w*' see DISP*w*); T*w* and G*w*, global indices of size and symmetry weighted by property *w*. GETAWAY: ISH, standardized information content on the leverage equality; HIC, mean information content on the leverage magnitude; H*kw* and R*kw*, H (molecular influence matrix; MIM) and R (MIM/distance matrix) autocorrelation descriptors of lag *k* weighted by property *w*; lag *k* refers to the number of edges in the fragment unit considered in the computation (for '*w*' see DISP*w*); HT*u*, H total index unweighted; HATS*kw*, leverage-weighted autocorrelation of lag *k* weighted by property *w*; R*kw*+, R maximal autocorrelation of lag *k* weighted by property *w*; see ref 36. [b] MLR-like regression coefficient of three-component PLS model; (fc) is fraction contribution of the regression coefficient to the activity; order indicates the order of their significance in the PLS model; the constant term of PLS model is 10.328; number of compounds are 23.

Table 3. Predicted Activity of Descriptor Cluster and Random Test Sets (eight compounds each) of the Compounds of Table 1 and the Corresponding Statistics

	residuals[a]					
	desc clust[b]			random[c]		
compd	eq 1	eq 2	PLS	eq 1	eq 2	PLS
4a	−0.17	0.09	−0.45			
4b	−0.13	−0.32	−0.13			
4c				−0.31	−0.33	−0.36
4f	−0.17	−0.12	−0.34	−0.10	−0.07	−0.31
6c	0.15	0.17	−0.01			
6e				0.10	0.11	0.45
6g				−0.26	0.01	0.16
6h	−0.04	−0.11	0.01			
4br				0.33	0.24	0.25
4hr	0.30	0.39	0.50	0.43	0.46	0.33
5cr	−0.66	−0.26	−0.46			
6cr				0.12	−0.25	−0.16
6fr	0.14	0.30	0.21	0.11	0.19	0.30
r	0.851	0.874	0.929	0.818	0.891	0.894
Q^2	0.429	0.455	0.745	0.395	0.381	0.622
R^2_{Pred}	0.64	0.736	0.516	0.681	0.688	0.532
s	0.234	0.226	0.165	0.267	0.22	0.208
F	9.64	8.11	22.95	7.41	9.7	14.58

[a] Difference of observed and predicted −log MIC; each training set has 15 compounds. [b] Test set from the descriptors clustering. [c] Test set from random selection.

enhanced dimension and symmetries along their principal axis 1 and 3 are favorable for the activity. In comparison to these 10 descriptors, the remaining ones appear in lower order of significance to influence the activity of the compounds (Table 2; Figure 6). A brief description of all the 50 descriptors is given in Table 2.

Conclusion

This study has provided a rational approach for the development of novel antitubercular agents based on 2,3-dideoxy hex-2-enopyranoside from carbohydrate synthon 3,4,6-tri-*O*-acetyl-α-D-glucal (**1**). Employing the MBH reaction, we conveniently introduced alkyl/arylalkyl groups at C-3 of hexenopyranosides, leading to this new class of molecules. The synthesis is almost completely diastereoselective without the usage of any external chiral agents. The correlation of the activity of these analogues with the 3D-descriptors emanating from the minimum energy conformation of **5c** suggests its relevance to the antitubercular activity. The conformational space of the minimum energy structure from conformational analysis (**5c**) and the X-ray structure (**4dr**) differ in their C-3 substitution region (Figure 3). Collectively, the identified descriptors suggest in favor of compounds embedded with some degree of symmetry, compact conformational features, and closely placed geometric and electronegativity centers for enhanced antitubercular activity. The involvement of the directional WHIM descriptors in the correlations suggests the complex nature of interaction between the compounds and their target. The autocorrelation descriptors from GETAWAY suggest in favor of three-centered structural fragments. Among the high active compounds, **4d** has shown no toxicity. It is identified for further development.

Experimental Section

General Methods. All the reactions were monitored by warming the $CeSO_4$ (1% in 1 M H_2SO_4) sprayed precoated silica gel TLC plates at 100 °C. NMR spectra were recorded on Bruker Avance DPX 200 FT, Bruker Robotics, and Bruker DRX 300 spectrometers at 200, 300 (^{1}H) and 50, 75 MHz (^{13}C). For ^{13}C NMR, reference $CDCl_3$ appeared at 77.4 ppm, unless otherwise stated. Mass spectra were recorded on a JEOL SX 102/DA 6000 mass spectrometer
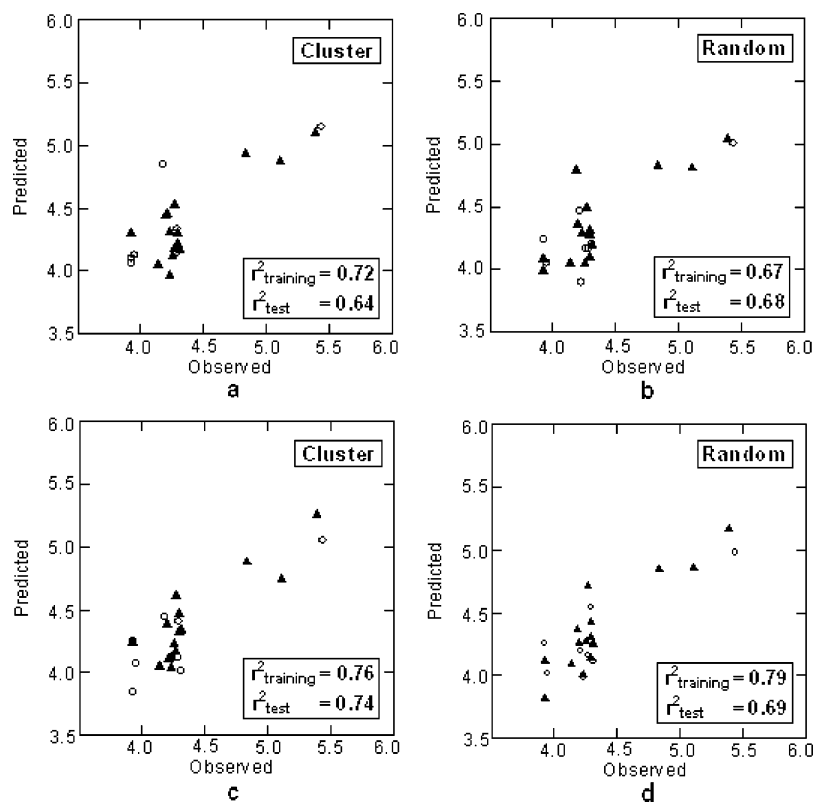
Figure 5. Plots of training (▲) and test sets (○) predicted activities versus observed activity corresponding to eqs 1 (a, b) and 2 (c, d). Number of compounds in training set is 15 and in test set is 8.
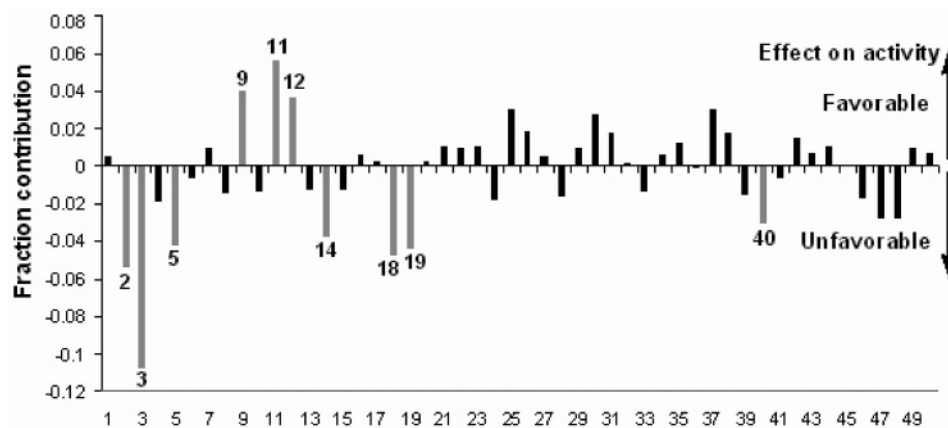

Figure 6. Plot of fraction contribution of MLR-like PLS coefficients (normalized) of the 50 descriptors (Table 2) to the activity. The horizontal axis refers to descriptors' serial numbers. The ten most significant descriptors are identified by gray shaded lines.

using argon/xenon (6 kV, 100 mA) as the FAB gas. IR spectra were recorded on Perkin−Elmer 881 and FTIR-8210 PC Shimadzu spectrophotometers. Optical rotations were determined on an Autopol III polarimeter using a 1 dm cell at 28 °C in methanol or chloroform as the solvent; concentrations mentioned are in g/100 mL. Elemental analyses were carried out on Carlo−Erba-1108 and Vario EL III instruments. A Bruker P4 diffractometer equipped with graphite monochromted Mo K_α radiation (0.71073 Å) at 293-(2) K was used for the X-ray Crystallographic study. *XSCANS* (Version 2.21. Siemens Analytical X-ray Instruments Inc., Madison, WI, 1996) was used for the data collection and reduction. *SHELXTL-NT* (Version 5.1. Bruker AXS Inc., Madison, WI, 1997) was used for structure refinement. Organic solvents were dried by standard methods. Aldehydes were purchased from Aldrich Chemical Co. and Fluka Chemical Co. Enones **4**, **5**, and **6** were synthesized in the lab.

General Procedure for the Preparation of 4a−6h. To a stirred solution of tetrabutylammonium iodide, TBAI (0.2 mmol), in dry CH_2Cl_2 (5 mL) at −78 °C was added $TiCl_4$ (1.5 mmol) dropwise.

After stirring for 2 min, a mixture containing enuloside **4**, **5**, or **6** (1 mmol) and the respective aldehyde (2 mmol) in dry CH_2Cl_2 (5 mL) was added. The reaction mixture was slowly warmed to −30 °C and stirred for the specified time depending on the enulosides and aldehydes used. A saturated aqueous solution of sodium bicarbonate was added, followed by filtration through a celite pad. The organic layer from the filtrate was separated, and the aqueous layer was again extracted with ethyl acetate. The organic layers were then combined, washed with brine solution, and dried over sodium sulfate. The crude product obtained after evaporation of the solvent was chromatographed to yield the pure compounds. Compounds **4a−c**, **4e−h**, **5c**, and **6c** are reported in previous publication.[44]

General Procedure for the Preparation of 4ar−6hr. To a stirred solution of **4a−6h** in ethanol (10 mL) were added $NaBH_4$ (0.5 mmole) and $CeCl_3·7H_2O$ (1 mmol), and the reaction mixture was stirred continuously at room temperature for the specified time depending on the compounds to be reduced. After completion of the reaction (TLC control), excess $NaBH_4$ was neutralized with

acetone, and the reaction mixture was concentrated in vacuo to get crude product which upon column chromatography yielded the pure **4ar−6hr**. Compounds **4ar**, **4cr**, and **4hr** are reported in previous publication.[44]

Biological Activity. **Agar Dilution Method**.[46] Briefly, 2-fold serial dilutions of each test compound/drug were incorporated into 7H10 agar. Inoculum of *M. tuberculosis H$_{37}$Rv* was prepared from fresh Lowenstein−Jensen slants adjusted to 1 mg/mL (wet weight) in Tween 80 (0.05%) saline and diluted to 10^{-2} to give a concentration of approximately 10^7 cfu/mL. A 5 mL amount of bacterial suspension was spotted into 7H10 agar tubes containing 2-fold serial dilution of drugs per mL. The tubes were incubated at 37 °C, and final readings were recorded after 30 days. The MICs were read as the minimum concentration of drugs/compounds that completely inhibited the growth of *M. tuberculosis* per spot. Ofloxacin was used as the standard drug.

Cytotoxicity Studies. The cytotoxicity study was carried out in VERO cell line.[47] VERO cells, originally obtained from ATCC and maintained in CDRI, were seeded on a 96-well plate and incubated at 37 °C in 5% CO_2 and 95% air. Cells were exposed to varying concentrations (25, 50, 100 μg/mL) of the compound for 72 h. MTT [3-(4,5-dimethyl-2-thiazolyl)-2,5-diphenyl-2*H*-tetrazolium bromide] assay was performed as per the standard protocol to assess cell viability. It is based on the MTT reduction. Using the standard protocol, cytotoxicity was also studied in mouse macrophage cell line J 744A.1.[48]

QSAR Study. Dataset. Two structure databases of hexenopyranoside derivatives (Table 1), corresponding to the X-ray structure (**4dr**) and the minimum energy structure from the conformational analysis of a high active compound (**5c**), were created for the computation of molecular descriptors. The database structures of X-ray structure (**4dr**) were generated in MOE (molecular operating environment) software[54] by making appropriate changes to the crystal structure template followed by energy minimization in AM1 semiempirical method[55] (rms gradient 0.001) as implemented in the software to result in the final conformations. For the second structure database, the minimum energy conformation of **5c** was identified through its systematic conformational analysis in MOE with default parameter settings followed by energy minimization (force field: MMFF94)[56] and refinement of final conformation in AM1 method. The remaining structures of the database were generated from this template of **5c** by appending appropriate changes to it followed by structural refinement in AM1 method.

DRAGON software[36] was used for the computation of alignment free 3D-descriptors of the structure databases. This resulted in 681 and 679 descriptors, respectively, for the X-ray (**4dr**) and the minimum energy conformation (**5c**) structure databases. The antitubercular activity (MIC, in moles per liter) of the compounds (Table 1) was considered after its transformation into logarithm of the inverse of inhibitory concentration (−log MIC). The QSAR models were generated using CP-MLR[49] in conjunction with a three-stage descriptor classification protocol[50] and PLS analysis.[53]

CP-MLR. It is a 'filter'-based variable selection procedure for the model identification and development in QSAR studies.[49−51] It involves a combinatorial strategy with appropriately placed 'filters' interfaced with MLR and extracts diverse models having unique combination of descriptors from the dataset. The filters set the thresholds for the descriptors in terms of interparameter correlation cutoff limits in subset regressions (filter-1), *t*-values of the regression coefficients (filter-2), internal explanatory power (filter-3; square-root of adjusted multiple correlation coefficient of regression equation, r-bar), and the external consistency (filter-4; Q^2 i.e. cross-validated R^2 from the leave-one-out procedure). Throughout this study, for the filters-1, 2, and 4 the thresholds were assigned as 0.79, 2.0, and $0.3 \leq Q^2 \leq 1.0$, respectively. The filter-3 was assigned an initial value of 0.71. In order to collect the descriptors with higher information content, the threshold of filter-3 was successively incremented with increasing number of descriptors (per equation) by considering the r-bar value of the preceding optimum model as the new threshold for next generation.

Descriptor Classification Protocol. The three-stage descriptor classification protocol[50] is implemented with the two-descriptor combinations (baseline models), as they are the simplest to understand and explain the activity. In the first stage of the classification protocol, the correlations of the activity with two-descriptor combinations from the individual descriptor classes (DCs) of the dataset were used to sort the DCs into four categories. They are primary contributors (category I: a DC forms a model with its constituent descriptors), collective contributors (category II: a DC unable to form a model with its constituent descriptors, but forms model(s) in combination with a descriptor from another such DC), secondary contributors (category III: a DC forms a model(s) only in combination with category I) and noncontributors (category IV: a DC unable to form a model(s) in any manner like that of category I, II, or III). The sorted DCs were collated in the second stage to identify all the 3-descriptor models across the categories. In the last stage, the individual descriptors of all three-descriptor models were pooled to discover the higher models for the activity.

All the identified models were reassessed for chance correlations by repeated randomization of the activity.[51] Each identified model was subjected to 100 simulation runs with scrambled activity, and the emerging correlations were counted to express the percent chance correlation of the model under examination. The proposed models were validated through two test sets, one from the single linkage hierarchical clustering of all the descriptor of the compounds and the other from the random selection procedure, with each containing 8 out of 23 compounds in analysis. The descriptors identified in the CP-MLR were evaluated through the PLS procedure[53] as well.

Supporting Information Available: Characterization data for all new compounds **4br**, **4d**, **4dr**, **4fr**, **4er**, **5cr**, **6cr**, **6d**, **6e**, **6f**, **6fr**, **6g**, **6h**, and **6hr**; purity table showing elemental analyses of listed above compounds; ^{1}H NMR and ^{13}C NMR spectra of **4d**, **4dr**, **5c**, **5cr**, **6h**, and **6hr**; crystallographic information file (CIF) of **4dr**; molecular modeling coordinates of **5c**; complete data set of alignment free 3D-molecular descriptors of structure databases corresponding to the X-ray crystal structure of **4dr** and the minimum energy conformation of **5c**; PLS loadings, weights, and sensitivity of independent and dependent descriptors of PLS model. This material is available free of charge via the Internet at http://pubs.acs.org.

References

(1) (a) *WHO Tuberculosis Fact Sheet*, 2004. http://www.who.int/mediacentre/factsheets/fs104/en/. (b) *WHO Tuberculosis Fact Sheet*, 1998. http://www.who.int/gtb/publications/factsheet/index.htm.

(2) (a) Dolin, P. J.; Raviglione, M. C.; Kochi, A. Global tuberculosis incidence and mortality during 1990−2000. *Bull. WHO* **1994**, *72*, 213−220. (b) Daffe, M.; Draper, P. The envelope layers of mycobacteria with reference to their pathogenicity. *Adv. Microb. Physiol.* **1998**, *39*, 131−203.

(3) Dye, C.; Scheele, S.; Dolin, P.; Pathania, V.; Raviglione, M. C. Global burden of tuberculosis: Estimated incidence, prevalence, and mortality by country. *JAMA* **1999**, *282*, 677−686.

(4) Somoskovi, A.; Parsons, L. M.; Salfinger, M. The molecular basis of resistance to Isoniazid, Rifampin, and Pyrazinamide in Mycobacterium tuberculosis. *Respir. Res.* **2001**, *2*, 164−168.

(5) Khasnobis, S.; Escuyer, V. E.; Chatterjee, D. Emerging therapeutic targets in tuberculosis: Post-genomic era. *Expert Opin. Ther. Targets* **2002**, *6*, 21−40.

(6) Maddry, J. A.; Suling, W. J.; Reynolds, R. C. Glycosyltransferases as targets for inhibition of cell wall synthesis in M. tuberculosis and M. avium. *Res. Microbiol.* **1996**, *147*, 106−112.

(7) Reynolds, R. C.; Bansal, N.; Rose, J.; Friedrich, J.; Suling, W. J.; Maddry, J. A. Ethambutol−sugar hybrids as potential inhibitors of mycobacterial cell-wall biosynthesis. *Carbohydr. Res.* **1999**, *317*, 164−179.

(8) Jones, P. B.; Parrish, N. M.; Houston, T. A.; Stapon, A.; Bansal, N. P.; Dick, J. D.; Townsend, C. A. A new class of antituberculosis agents. *J. Med. Chem.* **2000**, *43*, 3304−3314.

(9) Pasqualoto, K. F. M.; Ferreira, E. I. An approach for the rational design of new antituberculosis agents. *Curr. Drug Targets* **2001**, *2*, 427−437.

(10) Teodori, E.; Dei, S.; Scapecchi, S.; Gualtieri, F. The medicinal chemistry of multidrug resistance (MDR) reversing drugs. *Il Farmaco* **2002**, *57*, 385−415.

(11) Frieden, T. R.; Sterling, T. R.; Munsiff, S. S.; Watt, C. J.; Dye, C. Tuberculosis. *Lancet* **2003**, *362*, 887−899.

(12) Smith, C. V.; Sharma, V.; Sacchettini, J. C. TB drug discovery: Addressing issues of persistence and resistance. *Tuberculosis* **2004**, *84*, 45−55.

(13) Bayles, K. W. The bactericidal action of penicillin: New clues to an unsolved mystery. *Trends Microbiol.* **2000**, *8*, 274−278.

(14) Katz, A. H.; Caufield, C. E. Structure-based design approaches to cell wall biosynthesis inhibitors. *Curr. Pharm. Des.* **2003**, *9*, 857−866.

(15) McNeil, M.; Wallner, S. J.; Hunter, S. W.; Brennan, P. J. Demonstration that the galactosyl and arabinosyl residues in the cell-wall arabinogalactan of *Mycobacterium leprae* and *Myobacterium tuberculosis* are furanoid. *Carbohydr. Res.* **1987**, *166*, 299−308.

(16) Daffe, M.; Brennan, P. J.; McNeil, M. Predominant structural features of the cell wall arabinogalactan of *Mycobacterium tuberculosis* as revealed through characterization of oligoglycosyl alditol fragments by gas chromatography/mass spectrometry and by ¹H and ¹³C NMR analyses. *J. Biol. Chem.* **1990**, *265*, 6734−6743.

(17) Lee, R. E.; Smith, M. D.; Nash, R. J.; Griffiths, R. C.; McNeil, M.; Grewal, R. K.; Yan, W.; Besra, G. S.; Brennan, P. J.; Fleet, G. W. J. Inhibition of UDP-Gal mutase and mycobacterial galactan biosynthesis by pyrrolidine analogues of galactofuranose. *Tetrahedron Lett.* **1997**, *38*, 6733−6736.

(18) (a) Pathak, A. K.; Pathak, V.; Seitz, L.; Maddry, J. A.; Gurcha, S. S.; Besra, G. S.; Suling, W. J.; Reynolds, R. C. Studies on (β,1→5) and (β,1→6) linked octyl Gal*f*disaccharides as substrates for mycobacterium galactosyltransferase activity. *Bioorg. Med. Chem.* **2001**, *9*, 3129−3143. (b) Pathak, A. K.; Pathak, V.; Maddry, J. A.; Suling, W. J.; Gurcha, S. S.; Besra, G. S.; Reynolds, R. C. Studies on α-(1→5) linked octyl arabinofuranosyl disaccharides for mycobacterial arabinosyl transferase activity. *Bioorg. Med. Chem.* **2001**, *9*, 3145−3151.

(19) Wen, X.; Crick, D. C.; Brennan, P. J.; Hultin, P. G. Analogues of the mycobacterial arabinogalactan linkage disaccharide as cell wall biosynthesis inhibitors. *Bioorg. Med. Chem.* **2003**, *11*, 3579−3587.

(20) Centrone, C. A.; Lowary, T. L. Sulfone and phosphinic acid analogs of decaprenolphosphoarabinose as potential anti-tuberculosis agents. *Bioorg. Med. Chem.* **2004**, *12*, 5495−5503.

(21) Cren, S.; Gurcha S. S.; Blake A. J.; Besra, G. S.; Thomas N. R. Synthesis and biological evaluation of new inhibitors of UDPGal*f* transferase-a key enzyme in *M. tuberculosis* cell wall biosynthesis. *Org. Biomol. Chem.* **2004**, *2*, 2418−2420.

(22) Pathak, R.; Shaw, A. K.; Bhaduri, A. P.; Chandrasekhar, K. V. G.; Srivastava, A.; Srivastava, K. K.; Chaturvedi, V.; Srivastava, R.; Srivastava, B. S.; Arora, S.; Sinha, S. Higher acyclic nitrogen containing deoxy sugar derivatives: A new lead in the generation of antimycobacterial chemotherapeutics. *Bioorg. Med. Chem.* **2002**, *10*, 1695−1702.

(23) Pathak, R.; Pant, C. S.; Shaw, A. K.; Bhaduri, A. P.; Gaikwad, A. N.; Sinha, S.; Srivastava, A.; Srivastava, K. K.; Chaturvedi, V.; Srivastava, R.; Srivastava, B. S. Baylis−Hillman Reaction: Convenient ascending syntheses and biological evaluation of acyclic deoxy monosaccharides as potential antimycobacterial agents. *Bioorg. Med. Chem.* **2002**, *10*, 3187−3196.

(24) Gupta, M. K.; Sagar, R.; Shaw, A. K.; Prabhakar, Y. S. CP-MLR directed QSAR studies on the antimycobacterial activity of functionalized alkenols−topological descriptors in modeling the activity. *Bioorg. Med. Chem.* **2005**, *13*, 343−351.

(25) (a) Couladouros, E. A.; Strongilos, A. T. Generation of libraries of pharmacophoric structures with increased complexity and diversity by employing polymorphic scaffolds. *Angew. Chem., Int. Ed.* **2002**, *41*, 3677−3680. (b) Georgiadis, M. P.; Couladouros, E. A.; Delitheos, A. K. Synthesis and antimicrobial properties of 2*H*-pyran-3(6*H*)-one derivatives and related compounds. *J. Pharm. Sci.* **1992**, *81*, 1126−1131.

(26) Todeschini, R.; Lasagni, M.; Marengo, E. New molecular descriptors for 2D and 3D structures theory: Part 1. *J. Chemom.* **1994**, *8*, 263−272.

(27) Silverman, B. D.; Platt, D. E. CoMMA: Comparative molecular moment analysis. 3D-QSAR without molecular superposition. *J. Med. Chem.* **1996**, *39*, 2129−2140.

(28) Silverman, B. D. Three-dimensional moments of molecular property fields. *J. Chem. Inf. Comput. Sci.* **2000**, *40*, 1470−1476.

(29) Pastor, M.; Cruciani, G.; McLay, I.; Pickett, S.; Clementi, S. Grid−independent descriptors (GRIND): a novel class of alignment-independent three-dimensional molecular descriptors. *J. Med. Chem.* **2000**, *3*, 3233−3243.

(30) Consonni, V.; Todeschini, R.; Pavan, M. Structure/response correlations and similarity/diversity analysis by GETAWAY descriptors. 1. Theory of the novel 3D molecular descriptors. *J. Chem. Inf. Comput. Sci.* **2002**, *42*, 682−692.

(31) Consonni, V.; Todeschini, R.; Pavan, M.; Gramatica, P. Structure/response correlations and similarity/diversity analysis by GETAWAY descriptors. 2. Application of the novel 3D molecular descriptors to QSAR/QSPR studies. *J. Chem. Inf. Comput. Sci.* **2002**, *42*, 693−705.

(32) Bagchi, M. C.; Maiti, B. C.; Mills, D.; Basak, S. C. Usefulness of graphical invariants in quantitative structure-activity correlations of tuberculostatic drugs of the isonicotinic acid hydrazide type. *J. Mol. Model.* **2004**, *10*, 102−111.

(33) Bagchi, M. C.; Mills, D.; Basak, S. C. Quantitative structure-activity relationship (QSAR) studies of quinolone antibacterials against M. fortuitum and M. smegmatis using theoretical molecular descriptors. *J. Mol. Model.* **2007**, *13*, 111−120.

(34) Cratteri, P.; Romanelli, M. N.; Cruciani, G.; Bonaccini, C.; Melani, F.; GRIND-derived pharmacophore model for a series of alpha-tropanyl derivative ligands of the sigma-2 receptor. *J. Comput.-Aided. Mol. Des.* **2004**, *18*, 361−374.

(35) Gonzalez, M. P.; Suarez, P. L.; Fall, Y.; Gomez, G. Quantitative structure-activity relationship studies of vitamin D receptor affinity for analogues of 1alpha,25-dihydroxyvitamin D3. 1: WHIM descriptors. *Bioorg. Med. Chem. Lett.* **2005**, *15*, 5165−5169.

(36) Todeschini, R.; Consonni, V. Dragon software (version 3.0−2003), Milano, Italy, and references cited therein. http://www.talete.mi.it.

(37) Roth, W.; Pigman, W. In *Methods in Carbohydrate Chemistry*; Whistler, R. L., Wolfrom, M. L., Eds.; Academic Press Inc.: New York, 1963; Vol. 11, pp 405−407.

(38) Ferrier, R. J. Substitution-with-allylic-rearrangement reactions of glycal derivatives. In *Topics in Current Chemistry*; Springer-Verlag: Berlin, 2001; Vol. 215, pp 153−175 and references cited therein.

(39) Prevost, N.; Rouessac, F. A novel route to pyrimidine isodideoxy-nucleosides via Michael-type addition on unsaturated modified sugars. *Synth. Commun. 27*, **1997**, 2325−2335.

(40) Fraser-Reid, B.; McLean, A.; Usherwood, E. W.; Yunker, M. Pyranosiduloses. II. The synthesis and properties of some alkyl 2,3-dideoxy-2-enopyranosid-4-uloses. *Can. J. Chem.* **1970**, *48*, 2877−2884.

(41) (a) Morita, K-i.; Suzuki, Z.; Hirose, H. A Tertiary phosphine-catalyzed reaction of acrylic compounds with aldehydes. *Bull. Chem. Soc. Jpn.* **1968**, *41*, 2815. (b) Baylis, A. B.; Hillman, M. E. D. German Patent 2155113, **1972**; *Chem. Abstr.* **1972**, *77*, 34174q.

(42) (a) Basavaiah, D.; Rao, A. J.; Satyanarayana, T. Recent advances in the Baylis-Hillman reaction and applications. *Chem. Rev.* **2003**, *103*, 811−891. (b) Langer, P. New strategies for the development of an asymmetric version of the Baylis-Hillman reaction *Angew. Chem., Int. Ed.* **2000**, *39*, 3049−3052. (c) Ciganek, E. The Catalyzed α-hydroxyalkylation and α-aminoalkylation of activated olefins (The Morita-Baylis-Hillman Reaction) In *Organic Reactions*; Paquette, L. A., Ed.; Wiley: New York; 1997; Vol. 51, pp 201−350. (d) Basavaiah, D.; Rao, P. D.; Hyma, R. S. The Baylis-Hillman reaction: A novel carbon-carbon bond forming reaction. *Tetrahedron* **1996**, *52*, 8001−8062. (e) Drewes, S. E.; Roos, G. H. P. Synthetic potential of the tertiary-amine-catalysed reaction of activated vinyl carbanions with aldehydes. *Tetrahedron* **1988**, *44*, 4653−4670.

(43) Pathak, R.; Shaw, A. K.; Bhaduri, A. P. Chain extension of acyclic sugar derivatives via the Baylis−Hillman reaction. *Tetrahedron* **2002**, *58*, 3535−3541.

(44) (a) Sagar, R.; Pant, C. S.; Pathak, R.; Shaw, A. K. A substrate controlled, very highly diastereoselective Morita−Baylis−Hillman reaction: A remote activation of the diastereofacial selectivity in the synthesis of C-3-branched deoxysugars. *Tetrahedron* **2004**, *60*, 11399−11406. (b) In 33a the MBH-adduct derived reduced products were reported as in *threo* conformation. Now they are revised as in *erytho* conformation based on the X-ray analysis of compound **4dr**. (c) Sagar, R., Saquib, M., Shaw, A. K., Gaikwad, A. N., Sinha, S. K., Srivastava, A., Chaturvedi, V., Manju, Y. K., Srivastava, R., Srivastava, B. S. C-3 Alkyl or arylalkyl substituted 2,3-dideoxy glucopyranosides and a process for preparation thereof. Indian Patent 0533DEL2006, Ref. No. 0210NF2005/IN, 2006.

(45) Cahn, R. S.; Ingold, C.; Prelog, V. Specification of molecular chirality. *Angew. Chem., Int. Ed. Engl.* **1966**, *5*, 385−415.

(46) Saito, H.; Tomioka, H.; Sato, K.; Emori, M.; Yamane, T.; Yamashita, K.; Hosoe, K.; Hidaka, T. In vitro antimycobacterial activities of newly synthesized benzoxazinorifamycins. *Antimicrob. Agents Chemother.* **1991**, *35*, 542−547.

(47) Cory, A. H.; Owen, T. C.; Barltrop, J. A. Use of an aqueous tetrazolium/formazan assay for cell growth assays in culture. *Cancer Commun.* **1991**, *3*, 207−212.

(48) Srivastava, R.; Deb, D. K.; Srivastava, K. K.; Locht, C.; Srivastava, B. S. Green fluorescent protein as a reporter in rapid screening of antituberculosis compounds *in vitro* and in macrophages. *Biochem. Biophys. Res. Commun.* **1998**, *253*, 431−436.

(49) Prabhakar, Y. S. A combinatorial approach to the variable selection in multiple linear regression analysis of Selwood *et al.* data set- A case study. *QSAR Comb. Sci.* **2003**, *22*, 583−595.

(50) Gupta, M. K.; Prabhakar, Y. S. Topological descriptors in modeling the antimalarial activity of 4-(3′,5′-disubstituted anilino)quinolines. *J. Chem. Inf. Model.* **2006**, *46*, 93−102.

(51) Prabhakar, Y. S.; Solomon, V. R.; Rawal, R. K.; Gupta, M. K.; Katti, S. B. CP-MLR/PLS directed structure-activity modeling of the hiv-1rt inhibitory activity of 2,3-diaryl-1,3-thiazolidin-4-ones. *QSAR Comb. Sci.* **2004**, *23*, 234−244.

(52) The accompanied statistics of the equation: n, r, Q^2, s, and F represent, respectively, the number of compounds, correlation coefficient, cross-validated R^2 from leave-one-out (LOO) procedure, standard error of the estimate, and F-test value of the regression. The values given in parentheses are the standard errors of the regression coefficients.

(53) Wold, S. Cross-validatory estimation of the number of components in factor and principal component models. *Technometrics* **1978**, *20*, 397−405.

(54) MOE: The Molecular Operating Environment from Chemical Computing Group Inc., 1255 University St., Suite 1600, Montreal, Quebec, Canada H3B 3X3. http://www.chemcomp.com.

(55) Dewar, M. J. S.; Zoebisch, E. G.; Healy, E. F.; Stewart, J. J. P. Development and use of quantum mechanical molecular models. 76. AM1: a new general purpose quantum mechanical molecular model. *J. Am. Chem. Soc.* **1985**, *107*, 3902−3909.

(56) Halgren, T. A. Merck molecular force field. I. Basis, form, scope, parameterization, and performance of MMFF94. *J. Comput. Chem.* **1996**, *17*, 490−519.

JM070110H